

# Exoplanet Imaging with a Phase-induced Amplitude Apodization Coronagraph III. Hybrid Approach: Optical Design and Diffraction Analysis

Eugene A. Pluzhnik<sup>1,6</sup>, Olivier Guyon<sup>1</sup>, Stephen T. Ridgway<sup>2</sup>, Frantz Martinache<sup>3</sup>, Robert A. Woodruff<sup>4</sup>, Celia Blain<sup>1</sup> and Raphael Galicher<sup>5</sup>

## ABSTRACT

Properly apodized pupils can deliver point spread functions (PSFs) free of Airy rings, and are suitable for high dynamical range imaging of extrasolar terrestrial planets (ETPs). To reach this goal, classical pupil apodization (CPA) unfortunately requires most of the light gathered by the telescope to be absorbed, resulting in poor throughput and low angular resolution. Phase-induced amplitude apodization (PIAA) of the telescope pupil (Guyon 2003) combines the advantages of classical pupil apodization (particularly low sensitivity to low order aberrations) with full throughput, no loss of angular resolution and little chromaticity, which makes it, theoretically, an extremely attractive coronagraph for direct imaging of ETPs. The two most challenging aspects of this technique are (1) the difficulty to polish the required optics shapes and (2) diffraction propagation effects which, because of their chromaticity, can decrease the spectral bandwidth of the coronagraph. We show that a properly designed hybrid system combining classical apodization with the PIAA technique can solve both problems simultaneously. For such a system, the optics shapes can be well within today's optics manufacturing capabilities, and the  $10^{-10}$  PSF contrast at  $\approx 1.5\lambda/D$  required for efficient imaging of ETPs can be maintained over the whole visible spectrum. This updated design of the PIAA coronagraph maintains the high performance of the earlier design, since only a small part of the light is lost in the classical apodizer(s).

*Subject headings:* direct exoplanet imaging, coronagraphy, apodization, pupil remapping, diffraction propagation, hybrid optical design

## 1. Introduction

An optical system capable of extremely high contrast imaging (about  $10^{-10}$ ) at separations comparable to the telescope's diffraction limit is critical for direct imaging of extrasolar terrestrial planets.

Properly apodized telescope pupils (Nisenson & Papaliolios 2001; Kasdin et al. 2003), or de-

signs derived from the classical Lyot coronagraph (Soummer et. al 2003; Kuchner et al. 2005) provide the appropriate contrast level. Unfortunately, they suffer from low throughput, ranging from 0.1 to 0.3, and large inner working angles (IWAs), above  $3\lambda/D$ . More efficient concepts, capable of near 100% throughput and  $\approx \lambda/D$  IWA exist (Roddier & Roddier 1997; Baudoz et al. 2000; Rouan et al. 2000). They however exhibit a reduced performance for off-axis rays, sufficiently strong to prevent high contrast on nearby partially resolved stars.

A recently proposed alternative to the "classical" pupil apodization (referred to as CPA in this work) is to geometrically remap the entrance pupil of the telescope into an apodized pupil (Guyon

<sup>1</sup>Subaru Telescope, National Astronomical Observatory of Japan, 650 North A'ohoku Place, Hilo, HI 96720, USA

<sup>2</sup>National Optical Astronomical Observatories

<sup>3</sup>Observatoire de Haute Provence

<sup>4</sup>Lockheed Martin Space Corporation

<sup>5</sup>Ecole Normale Supérieure, Paris, France

<sup>6</sup>Institute of Astronomy of Kharkov National University, Sumskaya 35, 61022 Kharkov, Ukraine

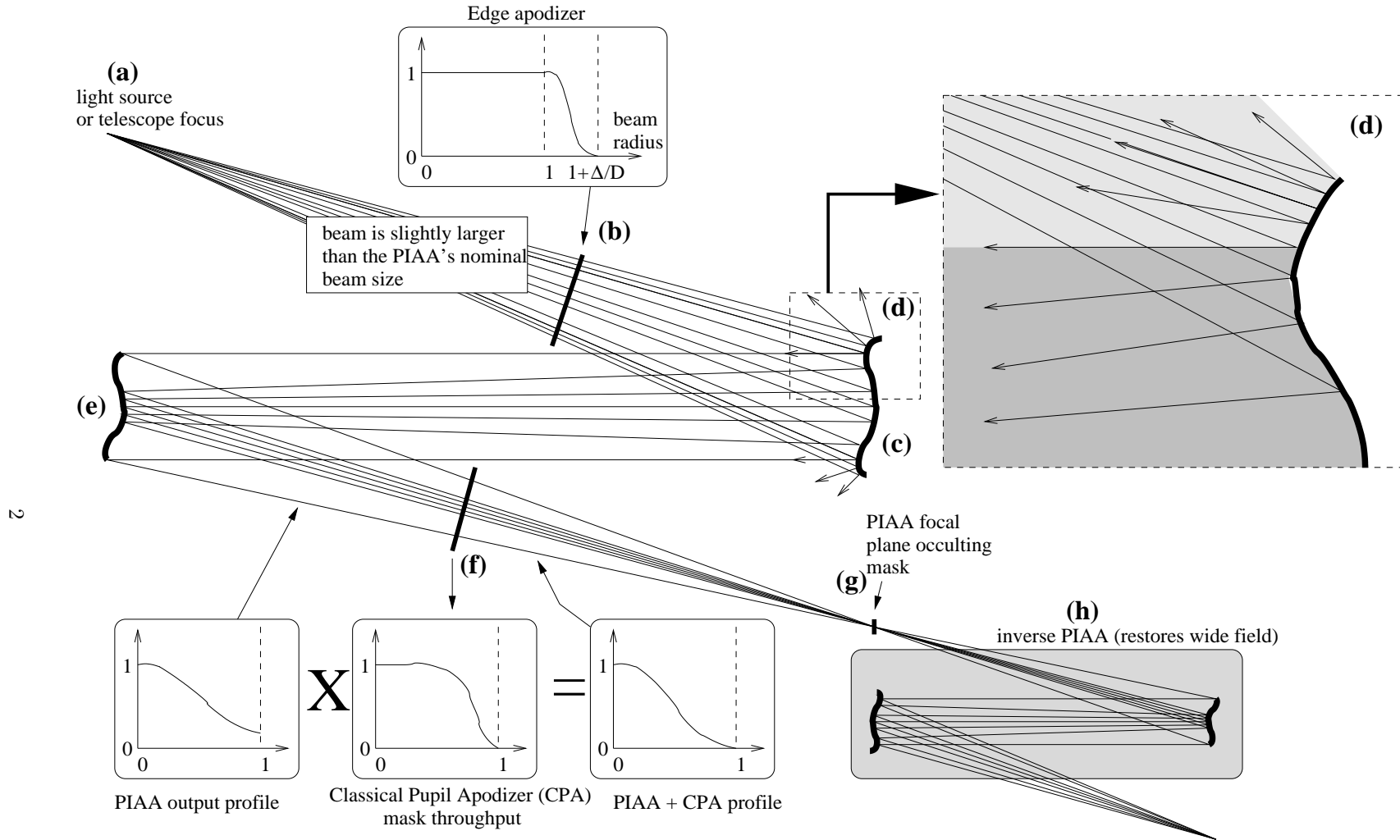


Fig. 1.— Optical layout of a PIAA/CPA hybrid Coronagraph. The system is shown with a focal plane input (a) and output (g), but could also be designed to accept and deliver a collimated beam. Most of the apodization is performed by the 2 aspheric mirrors M1 (c) and M2 (e), which remap the incoming beam into a truncated gaussian-like profile. A second apodization, produced by the classical apodizer (f), removes some of the light in the wings of this profile to produce a spheroidal prolate profile. The opaque focal plane mask (g) efficiently removes the light of the central source, while the rest of the field is fed to a PIAA unit mounted backwards (h) to restore a clean off-axis PSF over a “wide” field. In order to minimize unwanted diffraction effects, the apodization profile delivered by the aspheric mirrors is carefully chosen to avoid strong curvature on the M1 mirror. Further mitigation of diffraction effects is obtained by slightly oversizing the entrance beam and apodizing its outer edge (b). Thanks to a constant-curvature extension (d) of the first PIAA mirror, this oversized edge-apodized beam is projected on the second PIAA mirror (e) which therefore acts as the pupil stop in the system.

2003) (this technique is referred to as PIAA, or phase-induced amplitude apodization, in this work). This can be done with two aspheric optics, preferably mirrors: the first aspheric mirror is mostly used to project on the second mirror the desired beam profile, and the second mirror recollimates (or refocuses) the output beam. Mirror shapes can easily be computed by solving a differential equation (Guyon 2003; Traub & Vanderbei 2003). Although such a system corrupts the telescope isoplanaticity (the unaberrated field of view is only about of  $5\lambda/D$ <sup>7</sup>), a wide field of view can be restored by using the second set of post-coronagraphic PIAA optics (Guyon 2003) which does not affect the coronagraphic performance.

The PIAA technique combines many of the advantages found separately in other coronagraphs:

1. Very high throughput for the planet’s light (nearly 100%)
2. Small inner working angle (slightly larger than  $\lambda/D$ ).
3. Excellent achromaticity if implemented with mirrors (in the geometrical optics approximation).
4. Relative insensitivity to pointing errors.

These advantages have been quantified in several studies of the PIAA (Guyon 2003; Traub & Vanderbei 2003; Vanderbei & Traub 2005). A detailed analysis of a complete PIAA coronagraph (PIAAC) design was recently performed (Guyon et al. 2005), and the performance of the same design was evaluated for an imaging survey of ETPs with a space telescope (Martinache et al. 2005). This last study showed that the PIAAC is significantly more efficient than CPAs. A laboratory experiment, performed with lenses, has demonstrated beam apodization and imaging with a PIAA unit (Galicher et al. 2005).

While these studies showed that the PIAAC is, in theory, very efficient for direct imaging of ETPs, two serious concerns remain unanswered:

- **Optics manufacturability.** In the original PIAA design (Guyon 2003), the outer edge of the first PIAA mirror is highly curved. This feature, which is essential to obtain the desired apodization, is extremely difficult to polish.
- **Effects of diffraction propagation.** PIAA units have so far been designed and studied with geometric and Fraunhofer approximations. As recently shown by Vanderbei (2005), differences between diffraction propagation and geometric/Fraunhofer optics are not negligible at the  $10^{-10}$  contrast level.

In this work, we will address both issues through the study of a PIAA/CPA hybrid system. This new design combines a PIAA unit with a mild “classical” apodization of the beam. In §2, we focus on the optics manufacturability issue, present our hybrid design and explain how it solves this challenge.

In §3 we introduce the diffraction propagation problem in the PIAA apodizer and describe our method of diffraction calculation. The effects of diffraction propagation on the PSF contrast in a poorly designed system and possible solutions of the problem are analyzed in §4. Lessons learned from §4 are used to design a much superior hybrid system which is studied in §5. We give there a broader analysis of the PIAA design tradeoffs and quantify the performance of such systems for direct imaging of ETPs.

## 2. PIAA systems optical designs according to geometrical optics

### 2.1. PIAA unit design

In its original design, the PIAA optics consist of two aspherical mirrors M1 and M2 (Fig. 1). In the focus-to-focus system studied in this paper, the source is “collimated” by the first mirror M1 and reimaged by the second mirror M2.

The remapping function  $f(r_1)$  is determined in a such way that the total flux within the radius  $r_1$  of the input beam is equal to the total flux within the radius  $f(r_1)$  of the output beam. For any desired remapping function  $r_2 = f(r_1)$ , where  $r_1$  and  $r_2$  are the geometrical radii on mirrors M1 and M2 where a ray emitted by an on-axis

<sup>7</sup>Only the sky related angular scale  $\lambda/D$ , measured for the principal ray of the system (Guyon et al. 2005), is used in this paper.

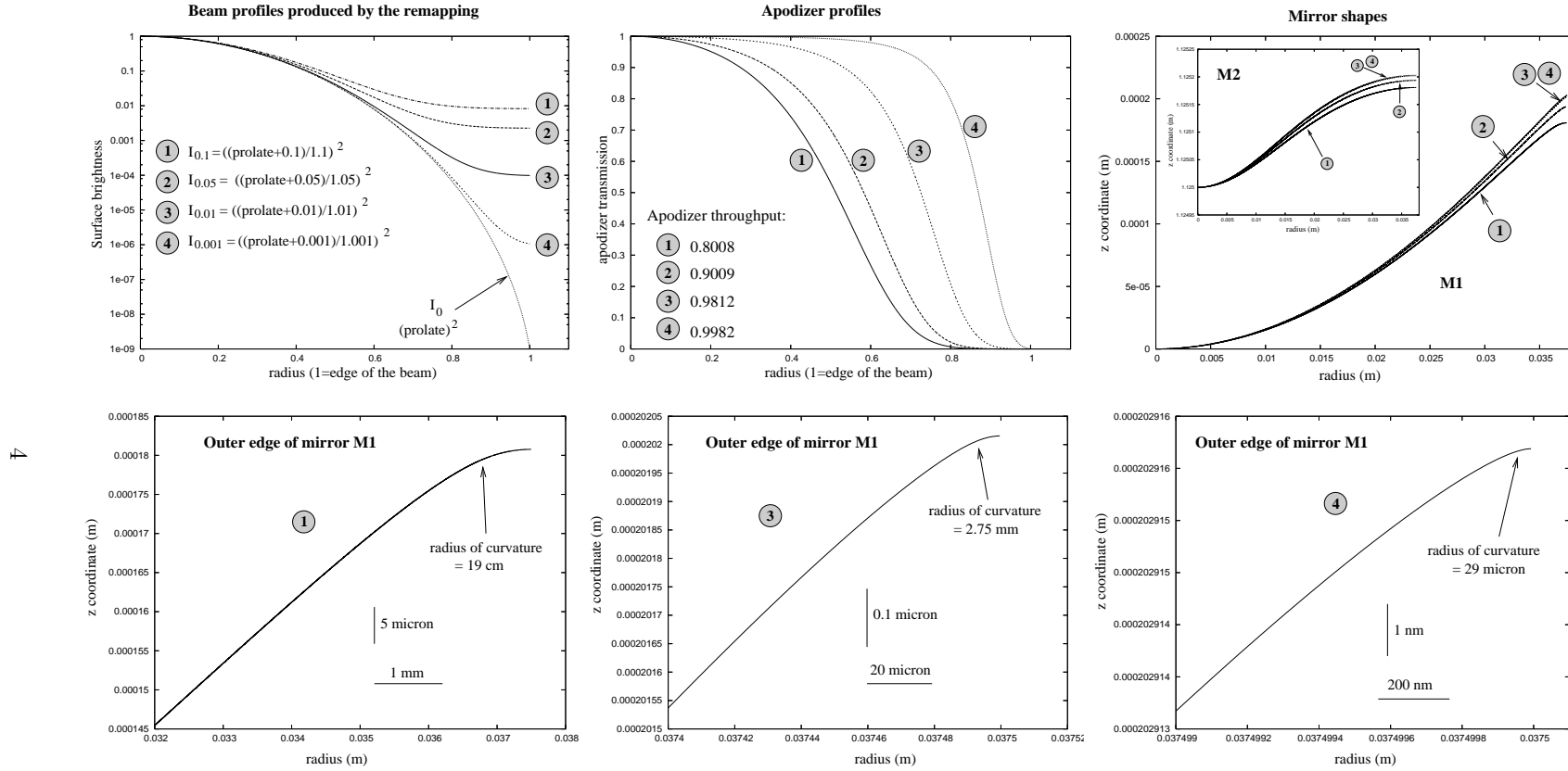


Fig. 2.— Surface brightness profiles  $I_\alpha$  for four values of  $\alpha$  (top left), and the prolate profile  $I_0$ . For each profile, the apodizer profile required to obtain the desired prolate beam is shown for an apodizer placed after the PIAA unit (top center). The aspheric terms in the mirror shapes are shown (top right) for M1 and M2. In the bottom panels, the shape of M1's edge is shown in more detail for three of the four values of  $\alpha$ .

source is reflected, the shape of the mirrors is obtained by solving the differential equation (Guyon 2003)

$$\frac{dM_1}{r_1} = \frac{dM_2}{r_2} = \sqrt{1 + \left(\frac{M_2 - M_1}{r_1 - r_2}\right)^2} - \frac{M_2 - M_1}{r_1 - r_2}, \quad (1)$$

and can be written as

$$M_i(r_i) = BP_i(r_i) + P_i(r_i). \quad (2)$$

In Eq. 2  $BP_i(r_i)$  is a paraboloid of rotation describing the base of the  $i$ -th mirror and  $P_i(r_i)$  describes the modification of the base shape to produce the desired apodization profile. The desired apodization profile is formed mainly by the first mirror M1, while the mirror M2 is mostly used to correct phase errors produced by the first mirror.

This first set of optics creates a properly apodized pupil beam which is used to form a high-contrast image. An occulting spot can then block the light of the central source. Off-axis aberrations introduced by the PIAA can be corrected by a second PIAA unit. The role of this second unit is only to “sharpen” the images of off-axis sources and it is therefore not discussed in this paper.

## 2.2. Optics shapes: the case for a hybrid PIAA/CPA approach

A prolate spheroidal beam amplitude profile can be shown to offer a contrast exceeding  $10^{-10}$  over a 360 degree search angle (Soummer et. al 2003). We denote  $I_0(r)$  its surface brightness profile. Unfortunately, this beam profile cannot realistically be obtained directly by remapping of the entrance pupil: the very faint outer edge of the prolate function (the profile edge to center brightness ratio is about of  $10^{-9}$ ) would require a “dilution” of the incombining beam’s edge by a factor approximately  $10^8$ : the outer 1% (in radius) of the apodized beam is to contain as much light as the outer  $10^{-8}\%$  of the unapodized beam. The optics shapes required to perform this task exhibit a narrow highly curved edge on the first mirror, which is both extremely challenging to manufacture and essential to reach the desired apodization in one step.

At least two solutions exist to mitigate this problem: splitting the remapping into several steps (this requires additional aspheric optical

elements) or sharing the apodization between a remapping system and a “classical” apodizer. This second option seems at present less costly and is adopted in this work. In this scheme, the manufacturability of the optics must be balanced against the overall throughput of the apodizer. Figure 2 illustrates four possible combinations, obtained by designing the pupil remapping unit to deliver a beam profile obtained by adding a constant  $\alpha$  to the prolate function:

$$I_\alpha(r) = \left(\frac{\sqrt{I_0(r)} + \alpha}{1.0 + \alpha}\right)^2. \quad (3)$$

The corresponding apodizer mask, required to produce the final beam profile  $I_0$ , is

$$T(r) = I_0(r)/I_\alpha(r) \quad (4)$$

and is also shown in Fig. 2. For higher values of  $\alpha$ , the throughput of the system is lower, but the optics become easier to manufacture (the outer edge of M1 becomes more gentle). Mirror shapes shown in Fig. 2 assume a 75 mm beam diameter on both M1 and M2 mirrors (referred to as the **working beam diameter**), a 1.125 m separation between M1 and M2, and a collimated input/output beam. With  $\alpha = 0.1$ , the system throughput is only 80%, but the M1 mirror shape is very “friendly”, with a 19cm minimum radius of curvature in the  $\approx 2$ mm wide outer edge. In a  $\alpha = 0.01$  system, only 2% of the light is lost in the classical apodizer, and the optics shape, although much more challenging, appears to be manufacturable (2.75mm minimum radius of curvature over the last  $\approx 20 \mu\text{m}$  of M1). With  $\alpha = 0.001$ , the throughput is excellent (99.8%) but M1 appears to be extremely difficult to manufacture: a well-controlled bend with a 29  $\mu\text{m}$  curvature radius over the last  $\approx 200 \text{ nm}$  of M1 would be required. Systems designed to require very little absorption by the apodizer are therefore very difficult to manufacture. We have not attempted to perform accurate geometrical and diffractive simulations for small values of  $\alpha$ , as the required number of sampling points for a such an analysis would be prohibitively high (for example, accurate simulation of a  $\alpha = 0.001$  system would require a  $\approx 5 \text{ nm}$  sampling at the outer edge of M1). For these reasons, our study is limited to systems that are both manufacturable and easy to simulate: systems for which the apodizer removes at least 1% of the flux.

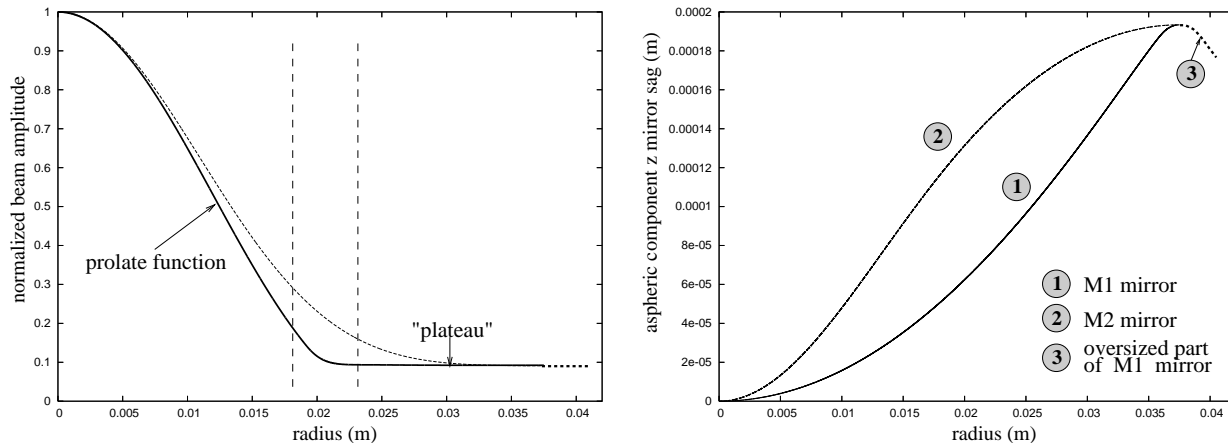


Fig. 3.— Shape of M1 and M2 mirrors (*right*) to produce the amplitude Profile I (*left, solid*) designed for our laboratory experiment. Only the aspheric terms in the mirror shapes are shown here. The two mirrors are separated by 1.125 m in the  $z$  direction. The amplitude profile  $\sqrt{I_{0.1}}(r)$  (*left, dashed*) is also shown for a comparison. Oversized parts of the working beam and M1 mirror are drawn with bold dashed lines.

In order to make mirror M1 easier to polish, the minimal surface brightness in the beam produced by the remapping optics needs to be kept above some level. The beam profile to be produced by the remapping optics does not have to be chosen according to Eq. 3. It is therefore tempting to design a remapping system with an output intensity profile that closely follows the  $I_0$  profile within the central region of the beam with a relatively quick transition to a “plateau” in the outer part of the beam. For the same “plateau” level, this new profile offers a throughput higher than the  $I_\alpha$  profile. An example of such a profile (Profile I) is shown in Fig.3 . This profile has been chosen for our upcoming laboratory experiment. In this paper it is used to demonstrate some diffraction effects encountered in a PIAA system. The central part of this profile is a prolate function continued with a constant level near the edge of the pupil.

Our hybrid PIAA/CPA apodization requires the use of an apodizing mask, just as a “classical” apodized pupil coronagraph does. Pupil apodizers for coronagraphs are technologically difficult to manufacture: the optical density needs to be well controlled and achromatic. Fortunately, the tolerances for the apodizer are easier to meet in the hybrid PIAA/CPA coronagraph than for a CPA coronagraph:

- In the PIAA/CPA design, the pre-apodizer

beam is already apodized, and the required maximal apodizer’s optical density is lower than if it were used without the PIAA.

- The apodizer only affects regions of the beam where the surface brightness is low. An error in optical density has therefore a smaller effect on the PSF contrast than if the apodizer were used by itself. In the central region of the beam the apodizer’s transmission is almost constant, and close to 100%. Large variations in the apodizer’s transmission only occur in the fainter outer parts of the remapped beam.

### 3. Diffraction propagation in a PIAA/CPA hybrid system

#### 3.1. Diffraction effects and PSF contrast chromaticity

Diffraction effects are most strongly introduced by discontinuities or sharp transitions. In a PIAA system, the outer edge of the beam (which could be defined by the edge of mirror M1) and the “sharp” bend near M1’s boundary are therefore of particular concern. While we will closely examine these effects and propose solutions to mitigate them in the following sections, we discuss here briefly their impact on the coronagraph performance.

Diffraction effects can modify the coronagraph behaviour, such that the coronagraph output is different from what geometrical optics theory predicts (Vanderbei 2005): the PIAA unit, as presented in §2.1, relies on geometrical optics to apodize the beam. As will be illustrated in the following sections, the difference between the expected (from geometrical optics) and actual (taking into account diffractive effects) apodized beams is quite small in most cases: less than  $\lambda/100$  RMS in phase in the visible. This difference is most likely not noticeable in practice, for two reasons:

- At this level of accuracy, a coronagraph optical system is relying on fine wavefront control rather than the intrinsic figure of the optics.
- The PIAA optics are manufactured as a set, one serving as the null for the other one. The diffraction effects therefore naturally occur during the testing of the optics: polishing to the null will compensate for the diffraction effects.

Even if the diffraction effects are significant, they can easily be integrated within the design of optical elements: residual phase errors can be projected on either M1 or M2; amplitude errors can also be cancelled by slight modification of M1's shape.

The first step of this process is to design the mirror shapes geometrically (Guyon 2003) to obtain the desired amplitude profile  $A_g(r)$ . The geometrically designed M1 mirror produces a diffraction pattern on the M2 surface with the OPD which is slightly different from the one predicted by geometrical optics laws. This difference can be corrected by changing of the M2 shape. For small incidence angles, the appropriate shape change is approximately  $(OPD_g - OPD_d)/2$  in  $z$  coordinate. We denote  $A_d(r)$  the output beam amplitude profile obtained by this OPD-corrected system. The resulting amplitude residuals can be then compensated by changing both M1 and M2 mirror shapes to geometrically produce an output beam with amplitude equal to  $A_g^2(r)/A_d(r)$ . A few iterations of this process rapidly converge to the solution for the mirror shapes with  $A_d(r) = A_g(r)$  when the diffraction effects are not very large. We

have successfully used a similar algorithm to design an off-axis focus-to-focus PIAA optical system, in which the optics shapes are non trivial, but can be obtained iteratively by correcting M1 and M2's shapes to cancel residual beam aberrations. In an hybrid PIAA/CPA system, amplitude aberrations can also be cancelled by the apodizer at a small cost in throughput.

A far more serious concern is the chromaticity of the diffraction effects: careful design of a PIAA/CPA system and/or fine correction by deformable mirror(s) can only cancel diffraction effects at a single wavelength. Strong diffraction effects therefore limit the spectral bandwidth over which the system can maintain an appropriate contrast. This is a general problem in high-contrast coronagraphy: mirror edges, mask edges and amplitude/phase aberration on optical elements all introduce wavelength-dependant effects through diffraction. For example, a pure optical pathlength difference (OPD) aberration will propagate (through diffraction propagation) into a chromatic OPD and amplitude aberration. While solutions to mitigate these problems in classical optical designs are relatively well known (oversizing optics which are not in a pupil plane, minimizing aberrations introduced by optics, conjugating DMs to the source of aberrations, etc...), it is largely unknown to what degree diffraction effects affect the PIAA system, and how to mitigate them.

The goal of this work is therefore to quantify the effect of diffraction propagation on the PSF contrast chromaticity and to identify solutions to mitigate it. Ultimately, we wish to verify if the PIAA coronagraph is truly achromatic, as geometrical optics predicts. All simulations presented in this work are for a PIAA/CPA hybrid design, which, unlike a pure PIAA system, seems manufacturable (see §2.2). In each optical configuration, it is assumed that the system is diffraction-compensated for  $\lambda_0 = 0.633\mu\text{m}$ : the PIAA unit optics shapes (and/or the DM shape) are such that no phase aberration is present at  $\lambda_0$ ; the classical apodizer is also designed such that no amplitude aberration is present at  $\lambda_0$ . We also assume that the PIAA optics shapes (and/or the DM) are achromatic: the OPD is independant of  $\lambda$ ; likewise, the throughput of the classical apodizer is assumed to be achromatic.

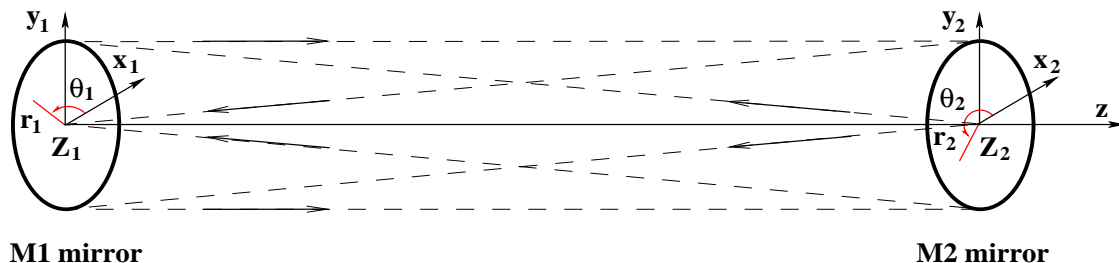


Fig. 4.— Geometry of the diffraction problem: A point source at  $Z_2$  in the center of mirror M2 is collimated by mirror M1, and then reimaged by M2 to  $Z_1$  at the center of M1.

### 3.2. Computation of the Rayleigh – Sommerfeld integral

For computational efficiency only symmetric, on-axis systems are studied in this paper. The geometry adopted for our diffraction computations is shown in Fig. 4. The  $z$  axis of the coordinate system passes through the centers of the mirrors M1 and M2. The centers  $Z_1$  and  $Z_2$  of M1 and M2 mirrors are at  $z_1 = 0$  mm and  $z_2 = 1125$  mm respectively. A point source is placed in the center  $Z_2$  of M2 mirror, while its image is formed in the center  $Z_1$  of M1 mirror (focus-to-focus system). Polar coordinates  $(r_1, \theta_1)$  and  $(r_2, \theta_2)$  are used to describe respectively M1 and M2 surfaces. The point source emits a spherical monochromatic wave which is reflected and diffracted by M1. The diffracted wave is focused by M2.

The full Rayleigh-Sommerfeld diffraction integral for propagation between two surfaces M1 and M2 is given by:

$$U(\mathbf{r}_2) = \frac{1}{\lambda} \int \int dx_1 dy_1 A(\mathbf{r}_1) e^{i\varphi(\mathbf{r}_1)} \left[ \frac{1}{kl} - i \right] \times \frac{M_2 - M_1}{l} \frac{\exp(ikl)}{l}, \quad (5)$$

where  $k = 2\pi/\lambda$ ,  $l = |\mathbf{r}_2 - \mathbf{r}_1|$ , and the point source emits a spherical monochromatic wave with amplitude  $A(\mathbf{r}_1) = A_0/\sqrt{r_1^2 + (z_2 - M_1)^2}$  and phase  $\varphi(\mathbf{r}_1) = 2\pi\sqrt{r_1^2 + (z_2 - M_1)^2}/\lambda$  on the surface of M1 mirror. In polar coordinates Eq. 5 can be written as

$$U(r_2) = \frac{2}{\lambda} \int_0^R A(r_1) e^{i\varphi(r_1)} (M_2 - M_1) r_1 dr_1 \int_0^\pi \left[ \frac{1}{kl} - i \right] \frac{\exp(ikl)}{l^2} d\theta_1, \quad (6)$$

where  $R$  is the mirror radius. Unfortunately, the accuracy of well known approximations for diffraction integrals (such as the Fresnel approximation) is not sufficient for coronagraphic applications (Vanderbei 2005). That is why we performed direct numerical integration of Eq. 6 to estimate the diffraction effects in the PIAA system by using a Fujitsu PrimePower2000 supercomputer at Subaru Telescope (Ogasawara et. al 2004). The supercomputer consist of 128 processors with the maximal performance of about 170 Gflops (Dongarra 2002). Calculation of the integral in Eq. 6 was performed for  $\lambda = 0.633\mu\text{m}$  and  $\lambda = 0.7\mu\text{m}$  with a sampling of about  $3R/\lambda$  (the step is equal  $2 \times 10^{-7}$  m) points in the radial direction and 10000 points in the angular direction. This sampling provides us with an accuracy in our diffraction calculation of about 0.05% in amplitude and  $2\pi/10^4$  radian in phase (Fig 5). These accuracy estimates are based on comparison of diffraction calculations with  $3.0R/\lambda$  radial  $\times$  10000 angular point and  $1.5R/\lambda$  radial  $\times$  20000 angular point sampling. The focal plane complex amplitude distribution was obtained by a discrete Hankel transform of the complex amplitude distribution on a reference sphere near the M2 mirror, assuming geometrical propagation between the mirror and the sphere.

### 4. Diffraction effects and possible solutions: examples from a poorly designed system

In this section, a PIAA/CPA hybrid system which has not been designed to mitigate diffraction propagation effects is studied. The design adopted, as will be demonstrated in this section, incorporates several bad choices, which makes it

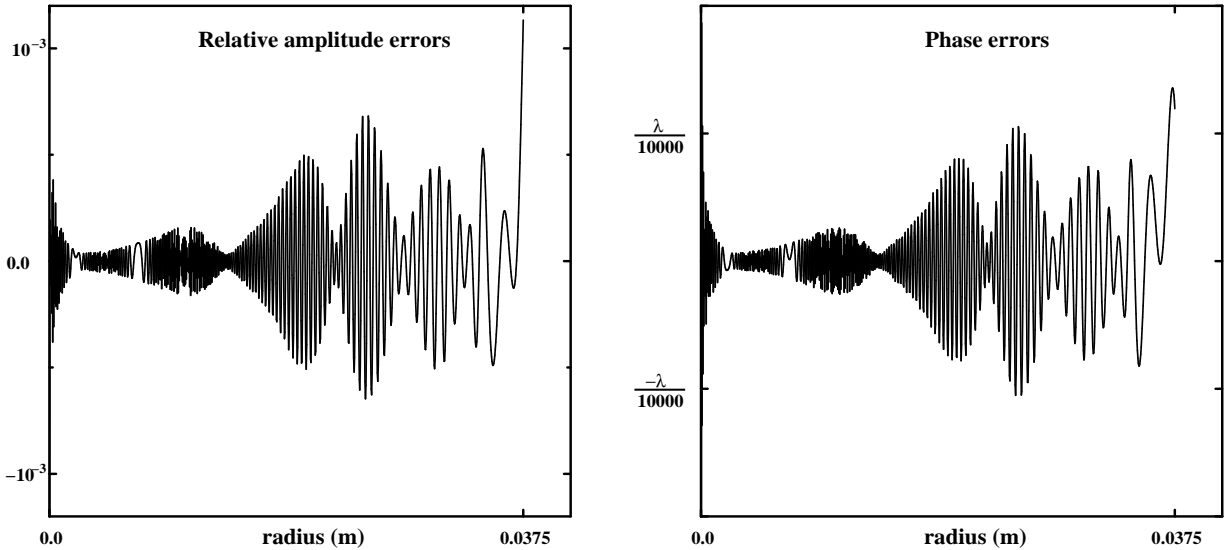


Fig. 5.— Relative amplitude difference and phase difference on the M2 mirror surface between diffraction calculation results obtained with two samplings, differing by a factor of 4.

inadequate for achromatic coronagraphy at the  $10^{-10}$  contrast level. It however provides us with a convenient example to illustrate the different diffraction propagation effects encountered, and explore solutions. Lessons learned from this exercise will be used in §5 to design a much superior PIAA/CPA system which is largely insensitive to diffraction propagation effects.

#### 4.1. Presentation of the design and diffraction through the system

The PIAA unit studied in this section is built to deliver a beam profile with a relatively sharp transition between an inner prolate spheroidal profile and a flat plateau at 0.1 times the peak amplitude (Fig. 3). A classical apodizer, placed downstream of the PIAA unit, then converts this profile into a pure prolate spheroidal, mostly by attenuating the “plateau”. In this system, a hard stop on M1 acts as a pupil stop. The size of this pupil stop is equal to the useful beam diameter.

Two diffraction features can be easily observed in the output beam (Fig. 6):

- High spatial frequency amplitude and phase oscillations getting stronger in the outer part of the beam.

- A large peak/hole in the center of the beam (the so called Arago spot).

Our diffraction propagation simulation shows that the PSF contrast at  $2\lambda/D$  in this system is  $10^{-7}$ . This PSF is shown in Fig. 7 and differs significantly from the PSF computed without diffraction propagation effects.

Because of their high spatial frequency and wavelength dependence, it seems to be difficult or impossible to correct the diffraction effects in a wide bandpass by using any combination of the PIAA mirror correction, a classical apodizer and/or a deformable mirror. A suitable method to control these diffraction features in the PIAA unit is considered below.

#### 4.2. Oversizing and edge apodization of the entrance beam

It should be noted that the diffraction features identified in §4.1 (high frequency oscillations and Arago spot) arise mainly from the sharp edge of the input beam (Rabinowicz 1965). The period and amplitude of these oscillations are decreasing when the distance from the edge of the beam is increasing. To reduce this effect, we now consider an M1 mirror with a radius 10% larger than the radius of the M2 mirror (Fig. 1, feature (d)). This

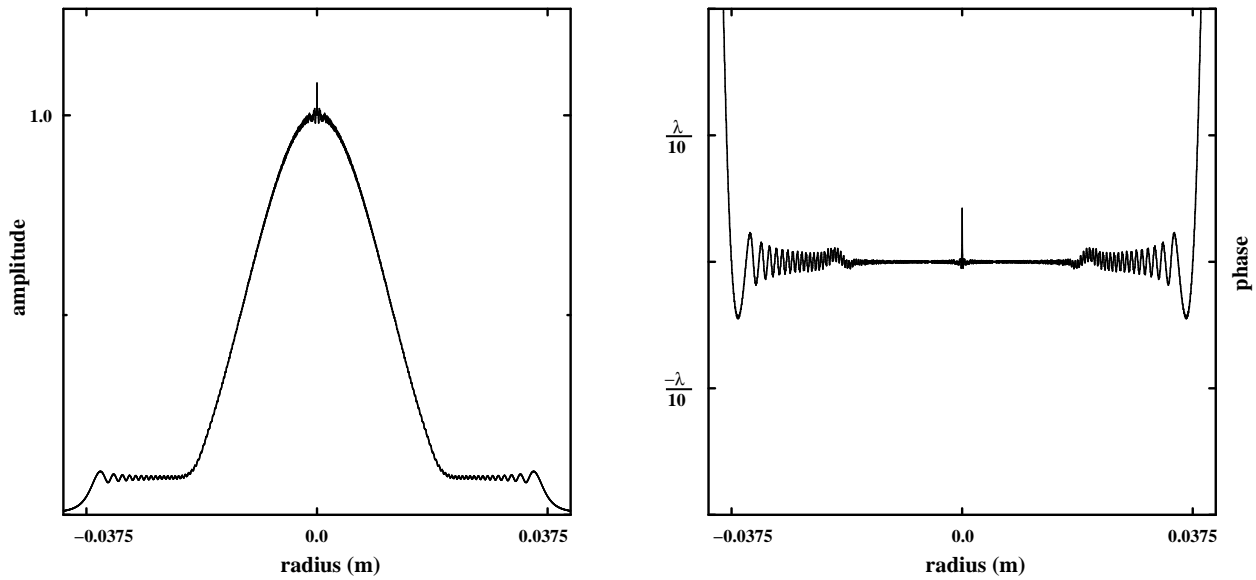


Fig. 6.— Diffraction effects in PIAA apodizer, prior to the classical apodizer. Amplitude and phase distributions on the surface of mirror M2 for the amplitude Profile I are shown here.

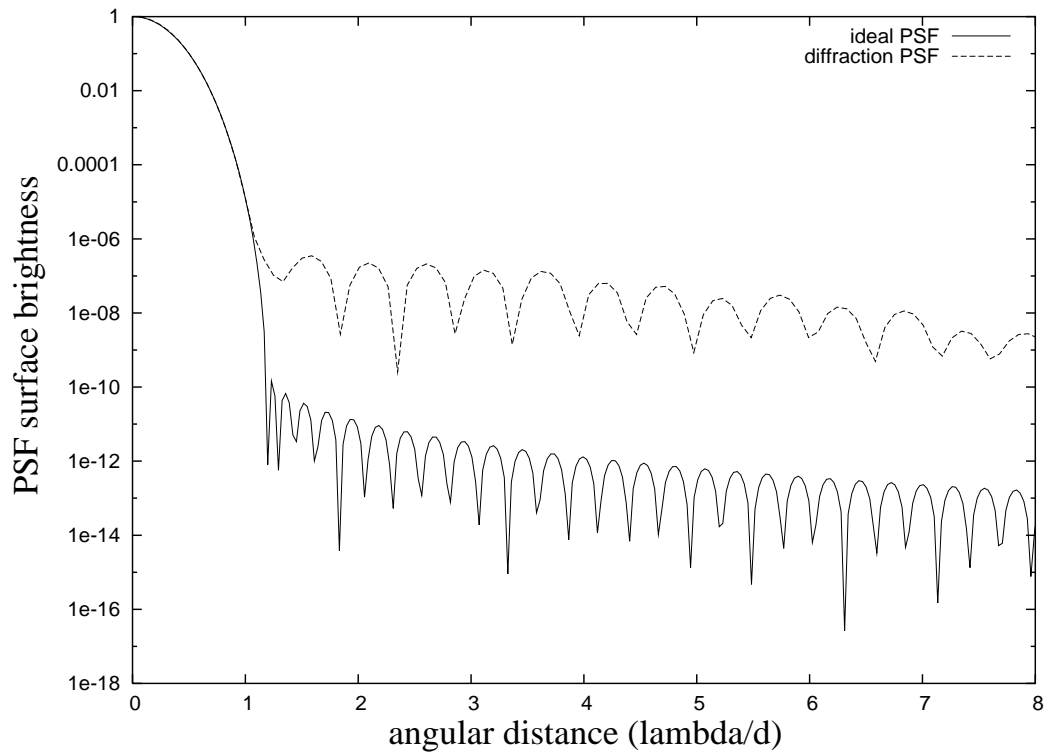


Fig. 7.— Diffraction effects in PIAA/CPA hybrid system based on amplitude Profile I: ideal and diffraction PSFs are shown. The system is designed to deliver  $10^{-10}$  contrast at  $1.5\lambda/D$  assuming geometrical optics laws.

”oversized” mirror is receiving an equally oversized beam. The shape of the M1 mirror is designed to continuously extend the input profile at a constant amplitude level outside the working aperture radius (dashed line in Fig. 3). Such a mirror still produces high frequency diffraction oscillations near the boundary of mirror M2 (Fig. 8), but they are now about 10 times smaller than the errors previously seen in the system without this mirror oversizing. Unfortunately, these diffraction features are still highly chromatic and relatively strong. Two methods to further reduce them can be proposed, namely:

1. using a carefully chosen edge apodizer for the M1 mirror;
2. using a destructive phase interference arising from toothed aperture at the M1 mirror (Shirley & Datla 1996).

Both edge apodizing and edge toothing can be performed outside of the working aperture and have no large effect on the optical design within the working aperture.

We choose here to implement solution (1) with a 10% cosine taper window to apodize the sharp edge of the “oversized” M1 mirror. Such an apodization smooths the beam edge within the 0.0375–0.04125 m radius interval and does not change the complex field within the working aperture. The diffracted field on the M2 surface for this “diffraction-free” system (Fig. 9) does not show either significant high frequency oscillations or the Arago effect. The maximal phase error is less than  $\lambda/150$  and rms of phase and amplitude errors are  $\lambda/780$  and 0.3% respectively.

#### 4.3. Toothed aperture

The use of sawtoothlike teeth on the edge of coronagraph occulting mask was first proposed by Purcell and Koomen (1962) to reduce flux diffracted into the shadow region behind the mask (corresponding to the working beam diameter here), and later proposed to reduce diffraction errors in radiometry (Boivin 1978). The method is based on the simple assumption that the radiation diffracted by a straight edge propagates in a direction perpendicular to it. According to this simple model no edge normal line should cross the “diffraction-free” region. For circular apertures,

the “diffraction-free” region is a circle of diameter depending on the number of teeth, the tooth depth and position of the “teeth” edge relative to the “diffraction-free” region. It is clear from simple geometrical considerations that the teeth should be placed at a small distance outside the working aperture. A simple diffraction description of this method has been given by Shirley & Datla (1996). We will present our results on this method in a following paper.

#### 4.4. Secondary diffraction effects in the PIAA system

With the boundary diffraction wave now successfully reduced to a small level, thanks to methods detailed in §4.2, the main remaining sources of diffraction effects are regions of M1 with strong localized curvature. These “localized curvature induced” (LCI) diffraction waves can be observed near the geometrical projection of strong M1 curvature regions on the M2 surface (corresponding to the “transition” where the profile rapidly shifts from prolate to constant in Fig. 8). Compared with the boundary diffraction wave encountered in §4.1 these waves are both smoother (no small scale features) and smaller in amplitude. In monochromatic light, they can be corrected with a DM (phase) and a classical apodizer (amplitude). Such a correction, unfortunately, is not perfect for other wavelengths: the stronger these secondary effects, the narrower we expect the bandpass suitable for high contrast imaging to be (Fig. 10, 11). The regions of the maximal curvature near the boundary of the M1 mirror are the most critical for diffraction propagation. Two main constraints can be used to design M1’s shape to minimize unwanted LCI diffraction errors:

1. the maximal curvature of the M1 mirror should be limited to an appropriate level. This maximal curvature constraint also makes the manufacturing of the PIAA optics easier.
2. the curvature should not be changing too fast and should reach its maximal value at the boundary of the working beam to avoid a local curvature maximum within the working beam diameter. In this case, LCI diffractive waves will be reduced due to destructive interference arising from the neighbor-

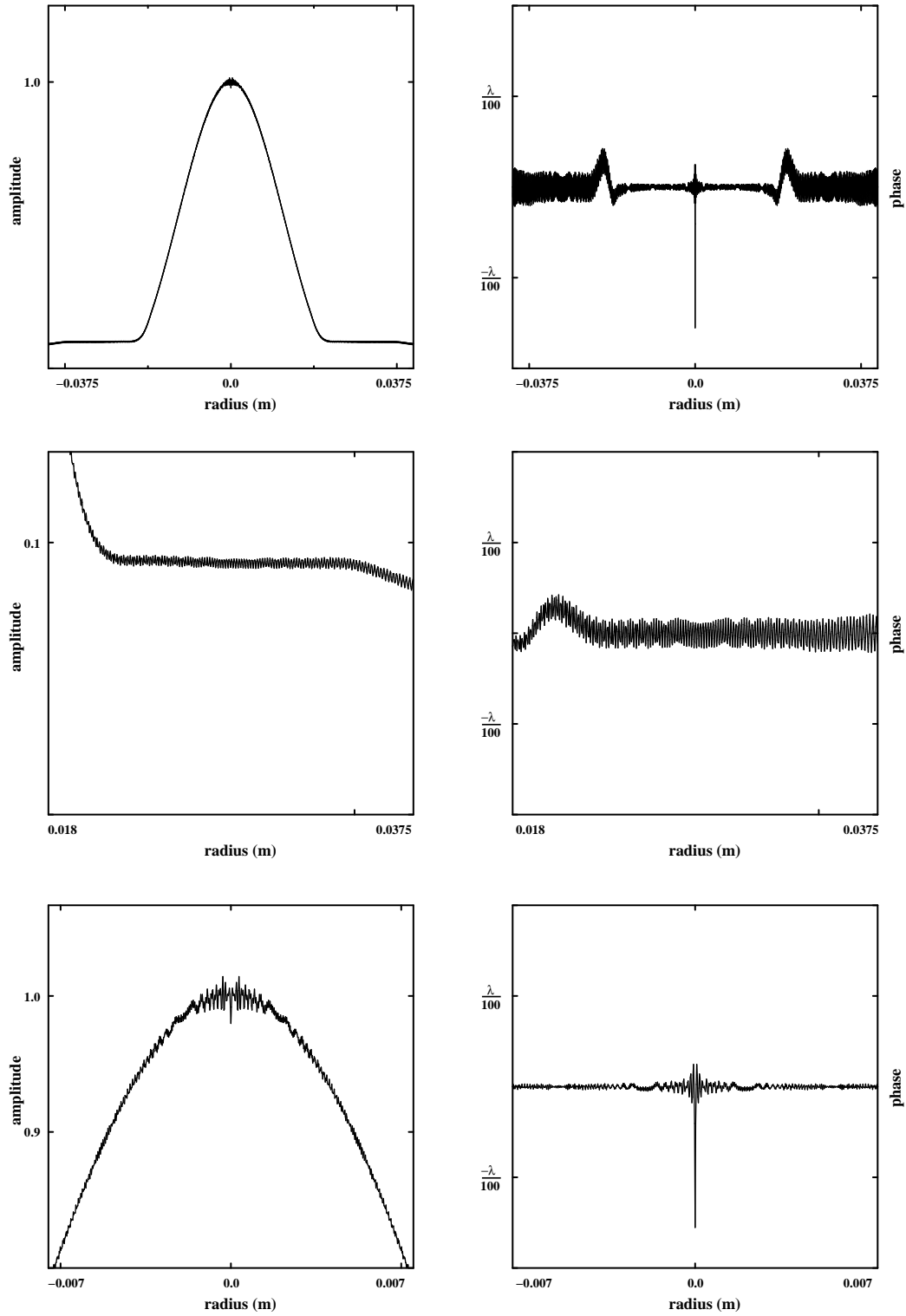


Fig. 8.— Diffraction effects in PIAA apodizer with an “oversized” beam. Amplitude and phase distributions on the surface of M2 mirror for amplitude Profile I are shown. The core and wings of the amplitude profile are presented separately in the second and the third rows.

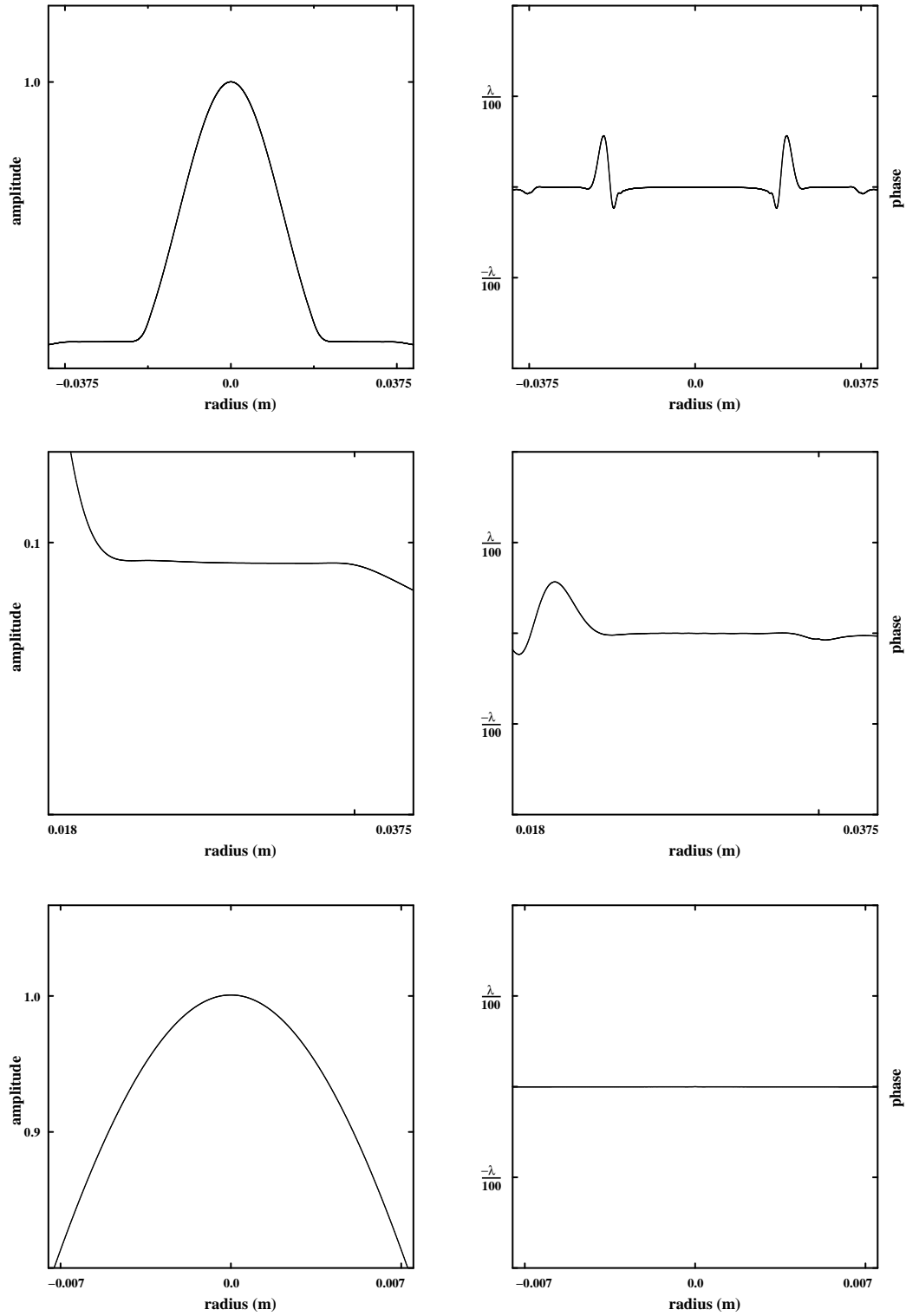


Fig. 9.— Diffraction effects in PIAA apodizer with an oversized and edge-apodized beam. Amplitude and phase distributions on the surface of M2 mirror for amplitude Profile I are shown. The core and wings of the amplitude profile are presented separately in the second and the third rows.

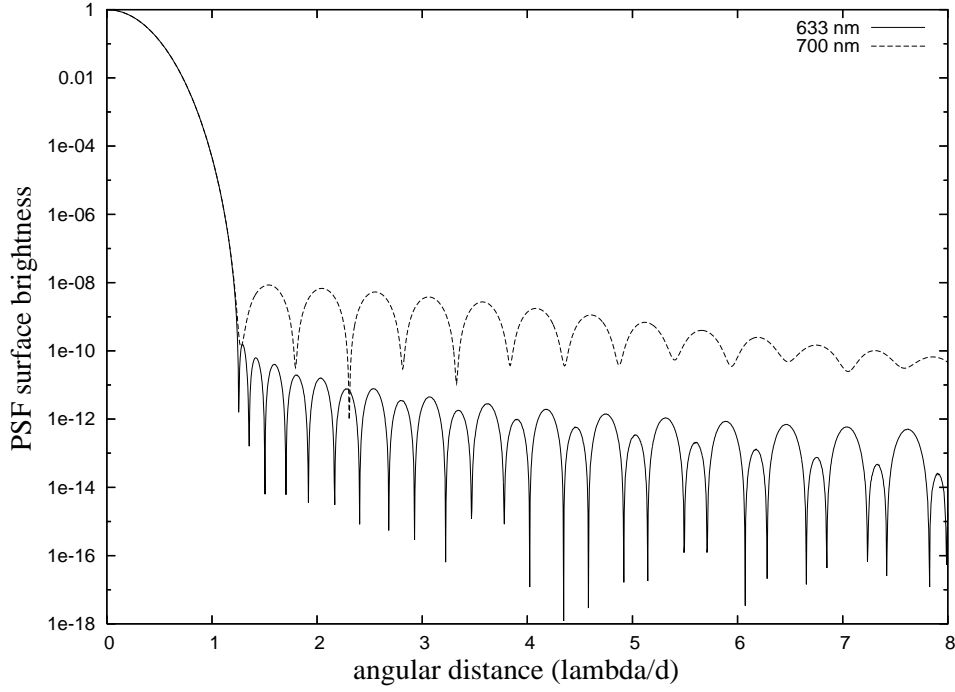


Fig. 10.— PSF chromaticity in a "diffraction-free" PIAA/CPA hybrid system utilizing a poorly designed PIAA unit. The PIAA unit, in this example, is built to deliver the amplitude Profile I. Both the amplitude profile and diffraction residuals are corrected to reach a  $10^{-10}$  contrast level at  $1.5\lambda/D$  for  $\lambda = 0.633\mu\text{m}$ .

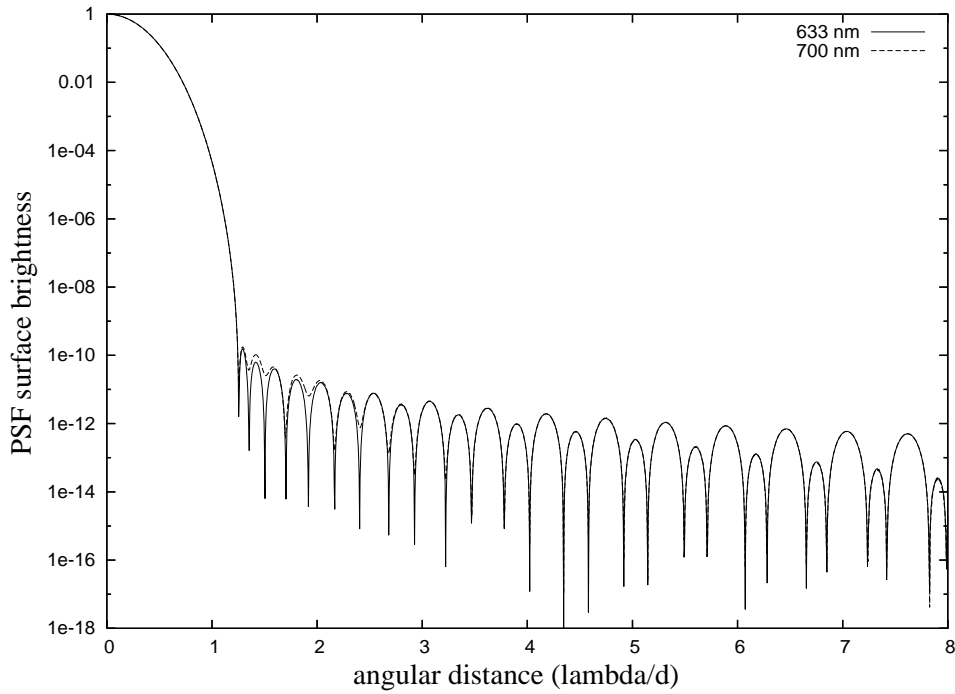


Fig. 11.— PSF chromaticity in a "diffraction-free" PIAA/CPA hybrid system utilizing a properly designed PIAA unit. The PIAA unit by itself, without the apodizers, is built to deliver the  $I_{0.1}$  beam profile. The PSF contrast is almost identical at  $0.633\mu\text{m}$  and  $0.7\mu\text{m}$ , suggesting that this design offers a very high level of achromaticity.

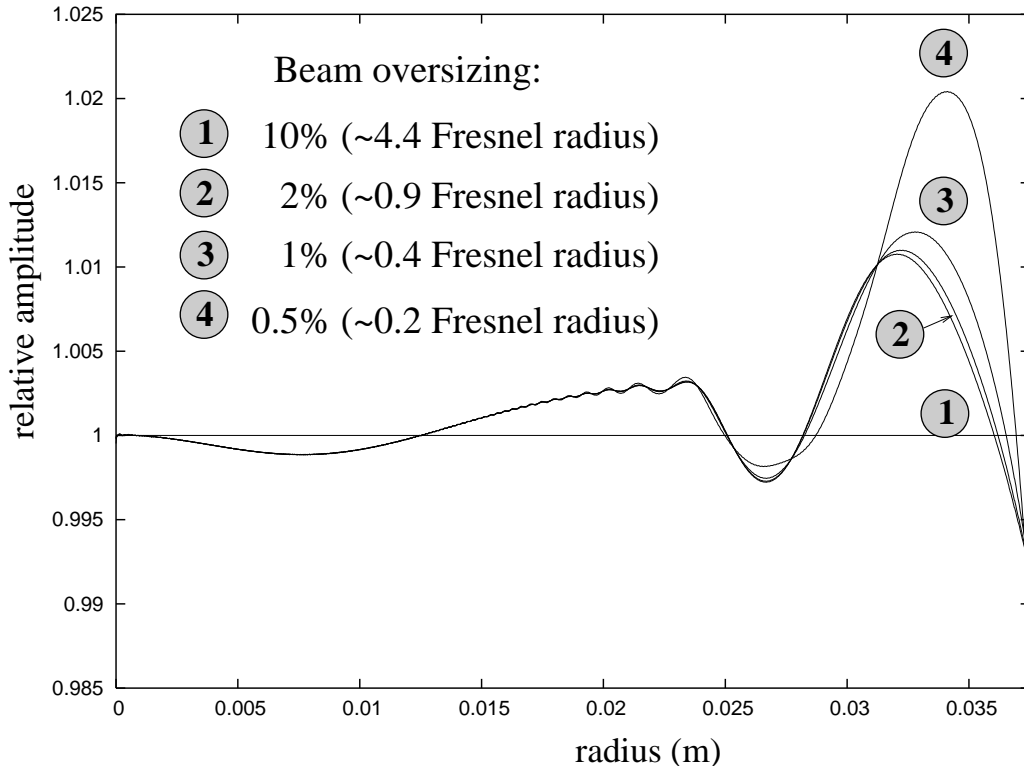


Fig. 12.— The combined LCI and boundary diffraction effects in a "diffraction-free" PIAA apodizer ( $\alpha = 0.03$ ). Relative amplitudes of the LCI waves and boundary wave residuals in the output beam are shown for different "oversizing" widths.

ing areas within the working aperture diameter, and the boundary diffraction wave can be corrected by suitable oversizing and edge apodizing of the beam.

In Fig. 10 and 11, PSFs for hybrid systems based on amplitude Profile I and intensity profile  $I_{0.1}$  are shown in two different wavelengths ( $0.633\mu\text{m}$  and  $0.7\mu\text{m}$ ). Both profiles have an identical intensity level in the beam's "plateau". The only difference is that the "transition" between the inner (gaussian like) and outer ("plateau") parts of the beam is more gentle for the intensity profile  $I_{0.1}$ . Results in Fig. 10 show that the steep transition from a prolate function in the beam to a constant level in the beam cannot provide us with the contrast  $10^{-10}$  into a wide bandpass. On the other hand, mirror shapes corresponding to the family of much smoother intensity profiles  $I_\alpha$  (Eq. 3) are good examples of PIAA optics with minimal diffraction effects (Fig. 11) and are suit-

able for high contrast imaging. We will therefore adopt these profiles in the rest of this paper.

## 5. Optimal coronagraph design and its performance

We have shown above that the diffraction propagation effects in the PIAA coronagraph depend on its optical design. Particularly important design parameters are the maximal mirror curvature (through the parameter  $\alpha$  in Eq. 3) and the width  $\Delta$  of the "oversized" part of the M1 mirror. The coronagraph throughput, resolution and, as a result, its performance are also determined by these parameters. In this section we discuss how to optimize the PIAA unit design, propose a possible solution and estimate its performance.

$\alpha$	Resolution ( $\lambda/D$ )	Throughput	$\Delta\lambda/\lambda$
0.03	0.96	0.91	0.074
0.05	0.93	0.86	0.21
0.1	0.88	0.76	$\sim 0.6$

Table 1: Angular resolution, total throughput and bandwidth for the PIAA/CPA hybrid system at  $\lambda = 0.633\mu\text{m}$ . Note the total throughput is slightly larger for a system with the edge apodizing mask affecting the working beam.

### 5.1. Optimal choice of the beam oversizing $\Delta$

Our proposed “diffraction free” design, shown in Fig. 1, gives us a way to get a “diffraction free” output beam by (1) confining of the boundary diffraction wave outside of the working beam diameter and (2) reducing its amplitude by edge apodization. The cost of such a solution is to reduce the coronagraph throughput (by a factor equal to the relative square of the “oversized” area) and resolution (by a factor  $1 + \Delta/D$ ). These losses can be noticeable if the width  $\Delta$  is large.

There are two possibilities to maintain both a high total throughput and high angular resolution in the PIAA system. The first is to use the smallest value of  $\Delta$  which still offers the required system contrast and bandpass. Suppose that the amplitude profile can be considered constant next to the beam boundary, with respect to the constant mirror curvature next to the M1 mirror edge. Taking into account that the boundary wave is formed in the narrow  $\sim \sqrt{\lambda(z_2 - z_1)}$  (width of the first Fresnel zone radius) boundary area next to the M1 mirror edge, the width of the minimal “oversized” area can be as small as  $\sim \sqrt{\lambda(z_2 - z_1)}$ . This estimate is supported by direct diffraction calculations. In Fig. 12 relative amplitudes of the LCI diffraction waves and the boundary wave residuals, related to different “oversizing” widths, are presented (for  $\alpha = 0.03$ ): they show that for  $\alpha$  at least larger than 0.03 the boundary wave residuals are negligible in comparison with the LCI diffraction wave amplitude if  $\Delta \geq \sqrt{\lambda(z_2 - z_1)}$ .

The second possibility is to use the edge apodizing mask (preapodizer) partially affecting the working beam. In this scheme, the functions of the pre-PIAA edge apodizer and the post-PIAA classical apodizer are shared that make it possible

to slightly increase total system throughput.

### 5.2. Contrast and bandpass dependence on $\alpha$

If the boundary wave is corrected, the system performance is determined by the LCI diffraction waves. For quite large values of  $\alpha$  ( $\sim 0.1$ ) the hybrid system based on geometric optics calculations only is sufficient to reach a  $10^{-10}$  contrast at  $2\lambda/D$ . The amplitude of the LCI waves is however higher for smaller values of  $\alpha$  (the M1 mirror curvature increases inside of the working beam radius). As a result for  $\alpha \leq 0.01$  the LCI waves become the main factor affecting the PIAA coronagraph contrast. To reach a  $10^{-10}$  contrast in this case, we should use a hybrid design which corrects not only amplitude but also phase diffraction residuals. These diffraction residuals are highly chromatic and can not be corrected simultaneously in a wide bandwidth. The bandwidth is seen to depend on  $\alpha$  (Table 1) and, consequently, on the system throughput. The final hybrid PIAA design should optimize the bandwidth and the total system throughput to reach maximal planet detectibility.

### 5.3. Suggested optical design

We are now ready to present a preliminary design for a hybrid PIAA/CPA coronagraph suitable for high contrast imaging of terrestrial planets.

The proposed system is shown in Fig. 1. The shapes of both PIAA mirrors (Fig. 2, Table 2) have been designed geometrically to provide us with the  $I_{0.05}$  output beam profile. This profile has been chosen by balancing total system throughput against bandpass centered at  $0.633\mu\text{m}$ . (We did not use a formal optimisation because of the cost in computer time and because it is not needed for demonstration of feasibility.) Although the  $I_{0.05}$  output beam profile corresponds to the contrast  $10^{-5}$  at  $1.5\lambda/D$  only (Fig. 14), the optics has only 5.7 cm minimal curvature radius at its edge and can be realistically manufactured now. The additional apodization is performed by a classical apodizer. This apodizer removes only 10% of the light to produce a spheroidal prolate designed for  $10^{-10}$  contrast at  $1.5\lambda/D$ . Taking into account diffraction for propagation between M1 and M2 mirrors the PSF contrast of the geometri-

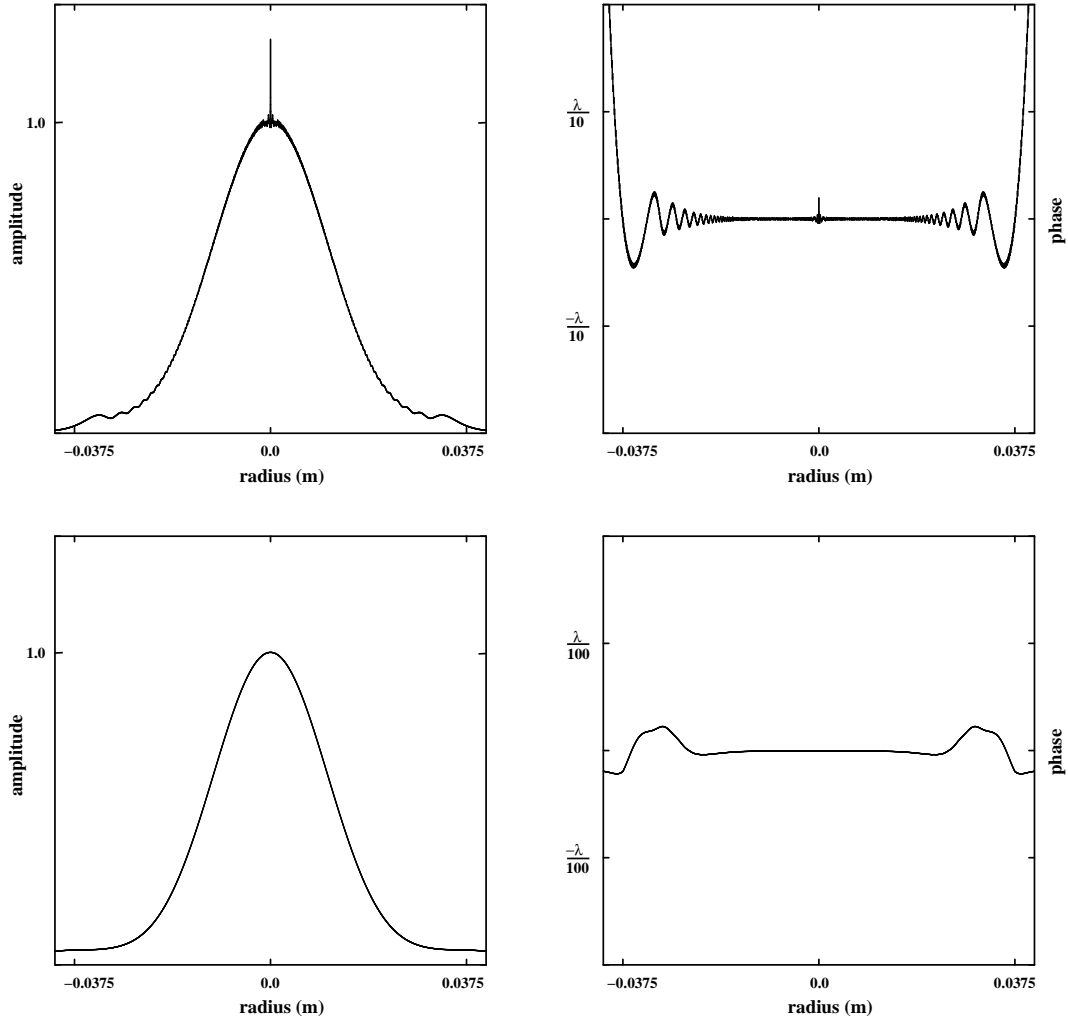


Fig. 13.— Suggested optical design: mitigation of diffraction effects in the PIAA apodizer. Amplitude and phase distributions on the surface of M2 mirror are shown for systems, based on the  $I_{0.05}$  intensity profile, without (*top*) and with (*bottom*) correction of diffraction effects.

$r$ , m	$P_1(r)$ , m	$P_2(r)$ , m
0.000000000	0.0000000000000000	1.1250000000000000
0.000000375	0.0000000000000021	1.1250000000000074
0.000000750	0.0000000000000087	1.1250000000000297

Table 2: Shape of M1 and M2 mirrors to produce  $I_{0.05}$  output beam intensity profile. The system is designed for a 1.125 m separation between mirrors and a collimated input/output beam. Columns (2) and (3) include  $P_1$  and  $P_2$  terms (Eq. 2) for each radius presented in column (1). The table is accessible in a machine-readable format.

cally designed system is limited to  $10^{-8}$  at  $1.5\lambda/D$  (Fig. 14). Mitigation of the M1 edge diffraction effects (Fig. 13) is obtained with only a 2% oversizing the entrance beam. The M1 mirror is designed to have a constant curvature into the oversized area, extended continuously from the working area. Fortunately, the mirror shape in the oversized area does not need to be of very high optical quality.

The oversizing width corresponds to the radius of the first Fresnel zone ( $\sqrt{\lambda(z_2 - z_1)}$ ) for propagation between the system mirrors and is responsible for a 4% loss in throughput and 2% loss in resolution. As a result the total throughput of the system is equal to 86%. The LCI diffraction effects in the proposed system are not more than 0.4% and  $\lambda/450$  in amplitude and phase respectively. They are small enough to keep the designed  $10^{-10}$  contrast at  $2\lambda/D$  into a 21% bandpass (Fig. 14).

It should be noted that the proposed design can be optimized for any designated spectral bandpass by a formal optimisation scheme.

#### 5.4. Performance of the hybrid PIAAC system for direct imaging of exoplanets

The PIAAC performance for direct detection of extrasolar planet has been studied by (Martinache et. al 2005). In this section, we use these results to estimate how a hybrid system would perform, based upon differences between our original PIAAC design (Guyon et al. 2005) and the design proposed in this work.

In our hybrid design, light from the edge of the pupil is lost by the two apodizers. The pre-mapping apodizer typically removes the outer 2% of the beam (4% of its area) to avoid edge diffraction effects. The post-mapping apodizer typically absorbs 2% of the light in a narrow-band

system ( $\alpha = 0.01$ ) to 10% of the light in a wide-band system ( $\alpha = 0.05$ ). As shown in Fig 2, the light lost due to this second apodizer is also mostly at the edge of the pupil. For the purpose of performance characterization, both apodizers can be approximated as edge-clipping masks, and we assume here that their combined effect is to absorb 10% of the total pupil surface (4% from the first apodizer, 6% from the second apodizer), or 5% of its radius. This estimate is conservative, since, as explained in §5.1, the functions of both apodizers may be combined to increase throughput.

The move from PIAAC to our hybrid design is therefore equivalent to a factor 0.93 in telescope diameter. A 4.3m diameter PIAAC hybrid telescope should perform as well as a 4m PIAAC telescope. We recall here the main findings of Martinache et al. (2005) with the telescope size adjusted for our new design:

- In only 70 s exposure (for 100% throughput telescope, no zodiacal/exozodiacal light), an Earth at 10 pc would have a 50% chance of being detected at the SNR=5 level.
- With a 4.3 m telescope, a quasi-complete detection survey of 100 F,G,K,M type stars for ETPs can be performed in about two days of “open shutter” observing time (100% throughput, 0.21  $\mu\text{m}$  bandwidth centered at 0.5  $\mu\text{m}$ , no zodiacal/exozodiacal light, 6 observations per star). This observing time should be distributed in at least a year to allow for the planets to orbit their parent stars.
- With more realistic assumptions (about 10% telescope+coronagraph+detector throughput), a survey of 200 stars for ETPs would require about one year of observation with a 4.3 m telescope.

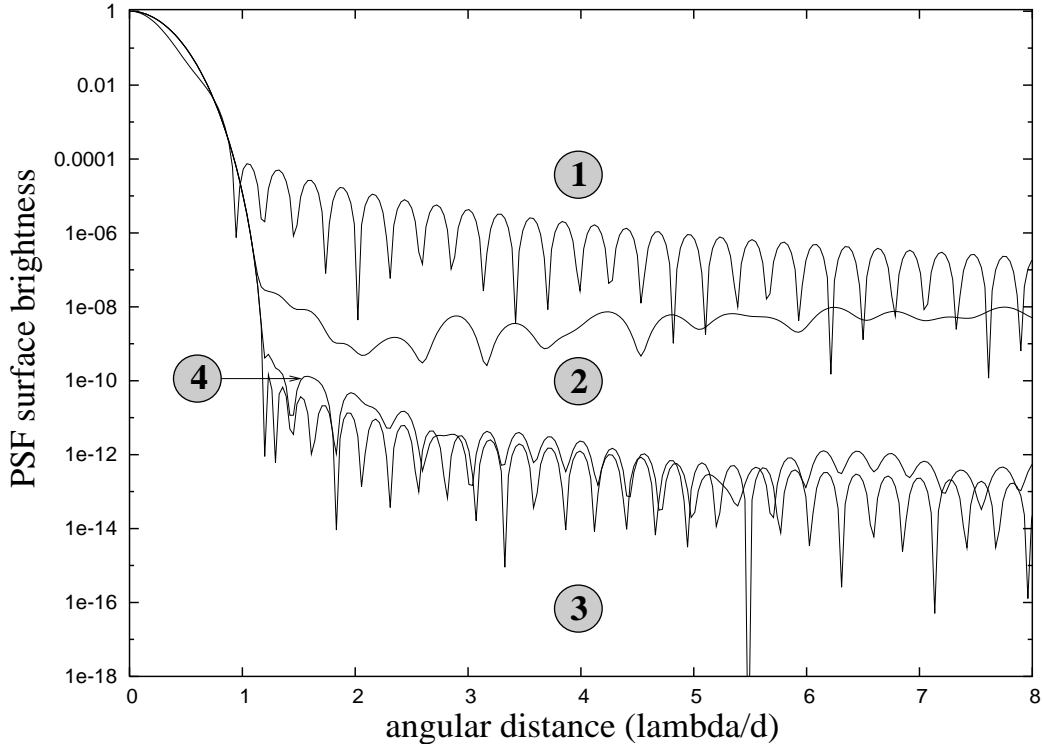


Fig. 14.— Suggested optical design: point spread functions. The PIAA unit is built to deliver only  $10^{-5}$  PSF contrast (1) by using  $I_{0.05}$  intensity profile. Because of diffraction, the hybrid PIAA/CPA system, (designed by assuming the geometrical optics laws) delivers only  $10^{-8}$  PSF contrast (2). The hybrid PIAA/CPA system designed by assuming the diffraction propagation ( $\lambda = 0.633\mu\text{m}$ ) keeps a  $10^{-10}$  contrast over 21% bandpass. The PSFs at  $\lambda = 0.633\mu\text{m}$  (3) and  $\lambda = 0.7\mu\text{m}$  (4) are shown.

- Thanks to the good angular resolution of the PIAAC hybrid, the impact of zodiacal + exozodiacal light is quite small (less than a factor of 2 in exposure time) for systems within 10 pc with less than 2 zodi observed with a 4.3 m visible telescope. Distant systems are however more strongly affected: the combined effect of a 2 zodi exozodiacal cloud and our zodiacal cloud is to multiply by 3.4 the required exposure time for a face-on system at 20 pc observed with a 4.3 m visible telescope.
- Even a 2.2 m visible telescope could detect Earth-tye planets around a few tens of stars.

## 6. Conclusion

Phase-induced amplitude apodization (PIAA) offers full throughput and small IWA, but the

required optics shapes are challenging to manufacture and the technique is prone to diffraction-induced chromatic effects. On the other hand, classical apodization coronagraphy is very robust, but suffers from low throughput and large IWA. We have shown in this work that both techniques can be combined in a “hybrid” coronagraph design to offer high coronagraphic performance (nearly 90% throughput,  $1.5\lambda/d$  IWA, low chromaticity) with “manufacturing-friendly” optics shapes.

The system presented in §5 achieves  $10^{-10}$  contrast at  $1.5 \lambda/d$  and beyond in a wide spectral band ( $d\lambda/\lambda \approx 0.21$ ) at a small cost in throughput (14%) and angular resolution (7%). Systems with higher throughput can be designed to operate in a smaller bandwidth.

The flexibility of our hybrid design leaves room for further optimization. For example, the roles

of the system's two apodizers can be shared to increase throughput. Ultimately, PSF contrast, spectral bandwidth, optics shapes and system throughput would need to be optimized for a particular telescope size and target list.

At the  $10^{-10}$  contrast level, small mirror figure errors (whether in OPD or reflectivity) introduce chromatic aberrations in the wavefront (Shaklan & Green 2005) which require the coronagraphic spectral bandwidth to be reduced to 10% or less. Our study therefore shows that a PIAA hybrid coronagraph can be designed to not be the dominant source of chromatic aberrations.

This work was carried out under JPL contract numbers 1254445 and 1257767 for Development of Technologies for the Terrestrial Planet Finder Mission, with the support and hospitality of the National Astronomical Observatory of Japan. The numerical computation has been carried on the Fujitsu PrimePower2000 supercomputer at Subaru Telescope, National Astronomical Observatory of Japan.

## REFERENCES

- Baudoz, P., Rabbia, Y., Gay, J. 2000, *A&AS*, 141, 319
- Boivin, L.P. 1978, *Apply Optics*, 17, 20, 3323.
- Dongarra, 2002, J.J. Technical Report CS-89-85, University of Tennessee, Computer Science Dept., July 7.
- Ebbets, D.C., Kilston, S., Linfield, R.P. 2003, in: *Proceeding of the SPIE*, 4860, 120.
- Galicher, R., Guyon, O., Otsubo, M., Suto, H., Ridgway, S.T. 2005, *PASP*, 117, 411.
- Guyon, O. 2003, *A&A*, 404, 379.
- Guyon, O., Pluzhnik, E.A., Galicher, R., Martinache, F., Ridgway, S.T., Woodruff, R.A. 2005, *ApJ*, 622, 744
- Kasdin, N.J., Vanderbei, R.J., Spergel, D.N., Littman, M.G 2003, *ApJ*, 582, 1147.
- Kuchner, M.J., Crepp, J., Ge, J. 2005, *ApJ*, 628, 466
- Martinache F., Guyon O., Ridgway S., Pluzhnik E., Galicher R., Woodruff R., 2005, accepted in *ApJ*.
- Nisenson, P., & Papaliolios, C. 2001, *ApJ*, 548, L201.
- Ogasawara, R., Kosugi, G., Takata, T., Mizumoto, Yo., Yasuda, N., Yagi, M., Kawarai, K., Kawai, A. 2004, *Proc. of the SPIE*, 4844, 188.
- Purcell, J.D., Koomen M.J. *Coronagraph with Improved Scattered-Light Properties*, Report of NRL Progress, 1962 (U.S. GPO, Washington, D.C.,1962).
- Rabinowicz, A. 1965, *Progress in Optics*, 4, 331.
- Rouan, D., Riaud, P., Boccaletti, A., Clnet, Y., Labeyrie, A. 2000, *PASP*, 112, 1479
- Roddier, F., Roddier, C. 1997, *PASP*, 109, 815
- Shaklan, S.B., Green, J.J. 2005, submitted to *Appl. Opt.*
- Shirley, E.L., Datta, R.U. 1996, *J. Res. Natl. Inst. Stand. Technol.*, 101, 745.
- Soummer, R., Aime, C., Falloon, P. E. 2003, *A&A*, 397, 1161.
- Traub, W.A., Vanderbei, R.J. 2003, *ApJ*, 599, 695
- Vanderbei, R.J., Traub, W.A. 2005, *ApJ*, 626, 1079
- Vanderbei, R.J. 2005, *astro-ph/0506550*